Computational Aeroacoustics as Applied to the Diffraction of Sound by Cylindrical Bodies

M. M. S. Khan,* W. H. Brown,† and K. K. Ahuja‡
Lockheed-Georgia Company, Marietta, Georgia

The problem of the diffraction of sound by two-dimensional rigid cylindrical objects has been formulated in generalized curvilinear coordinates. The governing equations for the aeroacoustic field are derived by perturbing the unsteady Euler equations and then extracting the steady mean flow equations from them. The governing equations are then solved by an explicit, four-stage Runge-Kutta, time-marching, finite-volume numerical scheme. The scheme has been implemented with far-field radiation and time-accurate wall boundary conditions. The cases of diffraction by a knife edge and a cylinder have been computed and compared against their corresponding analytical solutions in order to demonstrate the prediction capability of the numerical scheme. The acoustic field resulting from the interaction of the incident, reflected, and diffracted fields has been predicted very well in both the shadow and the illuminated zones. The scheme has also been applied to compute the diffraction of plane waves as well as that of a monopole acoustic field by a GA(W)-1 airfoil.

I. Introduction

WHEN sound waves impinge upon large rigid obstacles in their path, the resultant aeroacoustic field comprises of the incident waves, the reflected waves, and the diffracted waves. The diffraction of sound waves in the shadow zone plays a key role in assessing the acoustic shielding capability of aerodynamic bodies and forms a problem of fundamental importance in the field of aeroacoustics. The various fluctuating quantities that describe the aeroacoustic field are governed by the Euler equations which are, of course, nonlinear. Even if the governing equations are linearized, it is extremely difficult to obtain analytical solutions in the cases of the realistic two-dimensional obstacles such as airfoils without some unacceptable drastic simplifications. The difficulty can be essentially attributed to the complexities associated with the treatment of the boundary conditions. These difficulties pertaining to the analytical solutions have been appreciated by many investigators[1-4] and have led to the emergence of a new field of computational aeroacoustics (CAA).

Progress in the methods of CAA has now advanced because of the considerable advances in the fields of computational fluid dynamics (CFD) and computer technology. The aim of both CFD and CAA is to find solutions to the practical problems numerically, but the main differences between the two lie in the nature of the problems one deals with and in the type of the information one wishes to obtain. CFD treats steady as well as unsteady problems, whereas all the CAA problems are, by definition, unsteady. In current CFD problems, interests are focused primarily on the flowfield in the immediate vicinity of an aerodynamic body, and the objectives are to determine aerodynamic quantities such as pressure distributions, skin friction, lift and drag, etc. On the other hand, in CAA problems, attention is directed to both the near-field acoustic vibrations and the far-field noise radiation away from the body, and the objectives are to find the directivity and the spectral characteristics of the acoustic field. Therefore, while the well-established techniques of CFD can be utilized in order to develop the CAA methods, these fundamental differences call for special considerations in the development of CAA numerical methods. Some of these considerations are described below.

A. Consideration of Extremely Low Amplitudes of Acoustic Waves

One possibility for the prediction of the aeroacoustic fields is to use the existing time-dependent Navier-Stokes codes developed by various investigators directly in order to obtain a complete solution in the time domain. The fluctuating quantities, then, could be extracted from the solution by subtracting the mean flow quantities. A similar method has been adopted by Fasel[5] in the numerical investigation of boundary-layer instability. However, in many cases, the amplitude of the acoustic waves is found to be very low ($p \sim 2 \times 10^{-5}$ N/m^2), which rules out this procedure due to the possible unacceptable contamination resulting from the accumulation of round-off and truncation errors. Thus, in the present work, the governing equations are formulated by extracting the mean flow quantities in order to normalize the terms governing the fluctuating quantities. The equations are not linearized, and all the terms governing the fluctuating quantities are retained in the normalized form.

B. Consideration of the High Frequencies of Acoustic Waves

In many cases, the frequencies one deals with are much higher than those of interest in CFD problems. In order to retain meaningful resolution in the time domain, very small time steps ($\Delta t \ll 2\pi/\omega$) are, therefore, desired. In most of the practical cases, this resolution demands a Courant number lower than unity. Therefore, until and unless adverse instability conditions prevail, expensive implicit methods can be ruled out. Explicit methods have been successfully employed by previous investigators[3,4] in connection with specific problems in CAA, and in the present work, an explicit time-marching method has therefore been employed.

C. Consideration of the Low Scales of Acoustic Waves

One of the important characteristic length parameters of interest in the propagation of acoustic waves is the wavelength λ of the waves. In addition, there are at least three other distinct length scales to be considered: 1) a, the characteristic dimension of the aerodynamic body, 2) h, the characteristic mesh size of the computational grid, and 3) l, the characteristic length scale describing the extent of the

Received May 23, 1986; presented as Paper 86-1879 at the AIAA 10th Aeroacoustics Conference, Seattle, WA, July 9-11, 1986; revision received Oct. 13, 1986.

*Scientist. Associate Member AIAA.
†Scientist.
‡Scientist. Senior Member AIAA.

truncated computational domain. These form three nondimensional length scale parameters that serve as the indicators of the accuracy of the solution. The wavelengths encountered in CAA are much lower in magnitude than those of interest in common CFD problems. Thus, in order to avoid unacceptable distortions of the solution, one must have $h \ll \lambda/2\pi$, in addition to having $h \ll a$ in the vicinity of the body. In other words, the entire computational domain must contain a sufficient number of grid points per wavelength at each location. Although the condition $(2\pi h/\lambda) \ll 1$ is necessary for the accuracy of the solution, it is not a sufficient indicator of the truncation error of discretization. This fact has been pointed out by Bayliss, Goldstein, and Turkel.[6] The reason is that the discretization error depends not only upon $(2\pi h/\lambda)$, but also upon the number of wavelengths in the computational domain, i.e., the nondimensional length scale $(2\pi l/\lambda)$. Bayliss et al.[6] have shown that for a simple Helmholtz equation with a second-order finite-difference code, one must choose the number of points in each direction to be $N = 0.8(2\pi l/\lambda)^{3/2}$ to achieve approximately 7% L^2 accuracy. These two requirements of accuracy are achieved in the present work by putting adequate constraints in the generation of the computational grid.

Besides these considerations, it is also desired that the computational method should be applicable to complex geometric configurations. Thus, in the present work, the governing equations for the aeroacoustic field are obtained in generalized curvilinear coordinates. For the solution of the equations, MacCormack's scheme has been used by Hariharan[4] to study the sound radiation from cylindrical inlets. However, an algorithm for solving Euler equations, which offers significant advantages over the MacCormack scheme, has been developed by Jameson et al.[7] The algorithm is based on an explicit Runge-Kutta time-stepping finite-volume procedure wherein the spatial terms are central-differenced and an artificial dissipation is added to stabilize the algorithm. In the present work, the applicability of the algorithm has been extended and demonstrated to solve the governing equations of the aeroacoustic field. In summary, the purpose of the present work is, therefore, three-fold: 1) to construct a versatile computational method in generalized curvilinear coordinates suited for the diffraction problems of aeroacoustics, 2) to demonstrate its prediction capability by testing it against some of the known analytical solutions—for this purpose, the problems of the diffraction of plane waves by a knife edge and by a cylinder have been computed—and 3) to apply the method to obtain the acoustic field solutions for some of the simple practical cases, such as the diffraction of plane waves and a monopole acoustic field by a GA(W)-1 airfoil.

II. Governing Equations of Aeroacoustic Field

The governing equations for the acoustic perturbations can be derived from the unsteady compressible Euler equations. Let ρ, p, (u,v), and E denote the density, pressure, velocity components, and total energy, respectively. Let ρ_∞ and a_∞ denote the freestream density and the speed of sound respectively and L_{ref} be a reference length dimension in the flow. The various flow variables are nondimensionalized as follows:

$$\rho = \rho^*/\rho_\infty, \qquad p = p^*/(\rho_\infty a_\infty^2)$$

$$(u,v) = (u^*,v^*)/a_\infty, \qquad E = E^*/a_\infty^2$$

$$(x,y) = (x^*,y^*)/L_{\text{ref}}, \qquad t = t^*/(L_{\text{ref}}/a_\infty)$$

Then, if the intertial Cartesian velocity components are retained as dependent flow variables, the two-dimensional unsteady Euler equations can be written (see e.g., Pulliam and Steger, Ref. 8) in generalized curvilinear coordinates (ξ,η) in a conservation law form as follows:

$$\frac{\partial (J\hat{q})}{\partial t} + \frac{\partial \hat{E}}{\partial \xi} + \frac{\partial \hat{F}}{\partial \eta} = 0 \tag{1}$$

where

$$\hat{q} = \begin{bmatrix} \rho \\ \rho u \\ \rho v \\ \rho E \end{bmatrix} \tag{2}$$

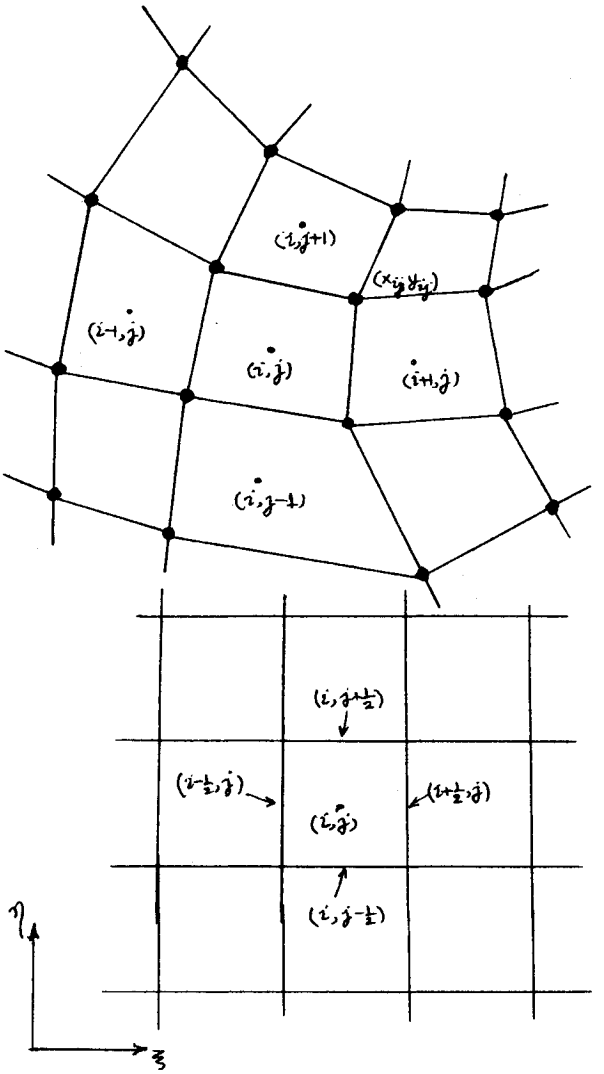

Fig. 1 Cell notations in the physical and computational domains.

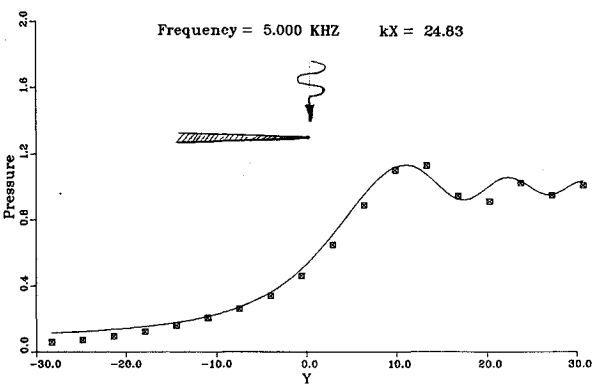

Fig. 2 Diffraction of the plane waves by a knife edge.

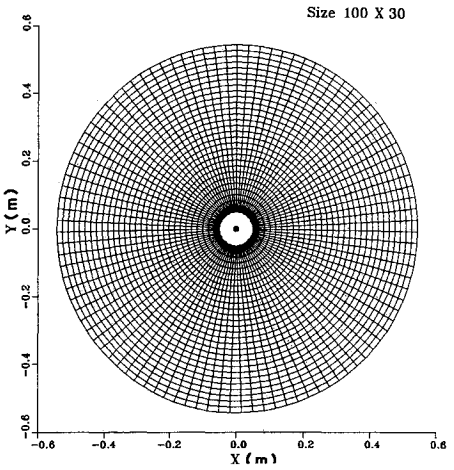

Fig. 3a The computational grid for a cylinder of diameter of 10 cm.

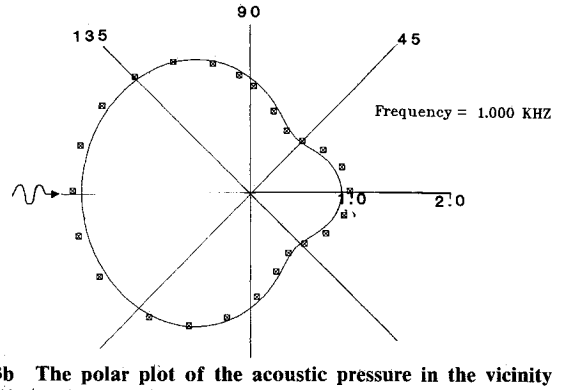

Fig. 3b The polar plot of the acoustic pressure in the vicinity of the cylinder ($kr=1.08$).

The inviscid flux terms are as follows:

$$\hat{E}=\begin{bmatrix} \rho U \\ \rho uU+y_\eta p \\ \rho vU-x_\eta p \\ (\rho E+p)U \end{bmatrix} \tag{3}$$

$$\hat{F}=\begin{bmatrix} \rho V \\ \rho uV-y_\xi p \\ \rho vV+y_\xi p \\ (\rho E+p)V \end{bmatrix} \tag{4}$$

where the contravariant velocities U, V are defined as follows:

$$U=y_\eta u-x_\eta v, \quad V=-y_\xi u+x_\xi v \tag{5}$$

and

$$J=x_\xi y_\eta - x_\eta y_\xi \tag{6}$$

The pressure can be obtained as follows:

$$p=(\gamma-1)[\rho E-\tfrac{1}{2}\rho(u^2+v^2)] \tag{7}$$

The complete Euler equations [Eqs. (1-7)], can be perturbed about a steady mean flow, first by substituting

$$\hat{q}=\hat{q}_0+a_q\hat{q}' \tag{8}$$

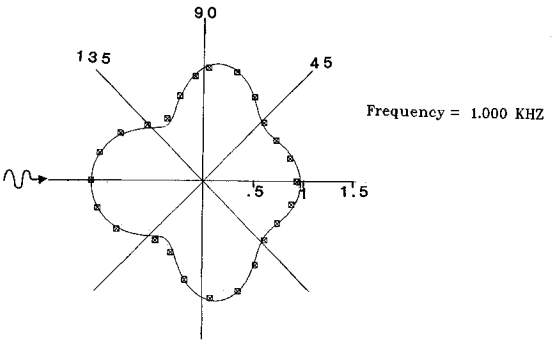

Fig. 3c The polar plot of the acoustic pressure around the cylinder at $kr=3.59$.

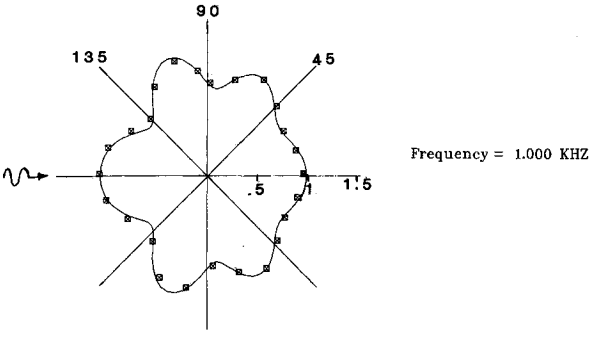

Fig. 3d The polar plot of the acoustic pressure around the cylinder at $kr=6.72$.

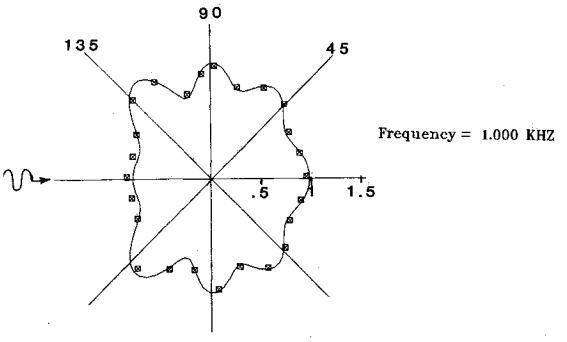

Fig. 3e The polar plot of the acoustic pressure around the cylinder at $kr=9.23$.

and then subtracting the steady equations governing the mean flow. Here the subscript 0 denotes the mean flow quantities and the primes denote the acoustic perturbation quantities. Also, a_q is the reference acoustic perturbation amplitude which, for example, can be taken as the standard acoustic reference pressure of 2×10^{-5} N/m^2. In other words, the amplitude a_q serves as the scaling parameters for the acoustic perturbations. Thus, the complete inviscid nonlinear equations governing the acoustic perturbations in the flowfield can be expressed in a generalized curvilinear coordinate system as follows:

$$\frac{\partial(J\hat{q}')}{\partial t}+\frac{\partial\hat{E}'}{\partial\xi}+\frac{\partial\hat{F}'}{\partial\eta}=S_a \tag{9}$$

where

$$\hat{q}'=\begin{bmatrix} \rho' \\ (\rho u)' \\ (\rho v)' \\ (\rho E)' \end{bmatrix} \tag{10}$$

and S_a represents any of the acoustic sources present in the flowfield. Defining the perturbed contravariant velocities as

$$(\rho U)' = y_\eta (\rho u)' - x_\eta (\rho v)'$$
$$(\rho V)' = -y_\xi (\rho u)' + x_\xi (\rho v)' \tag{11}$$

the perturbed inviscid flux terms can be written as follows:

$$\hat{E} = \begin{bmatrix} (\rho U)' \\ y_\eta p' \\ -x_\eta p' \\ 0 \end{bmatrix} + \frac{1}{(\rho_0 + a_q \rho')} \begin{bmatrix} 0 \\ [(\rho u)_0 + a_q (\rho u)'](\rho U)' \\ \quad + [(\rho u)' - (\rho'/\rho_0)(\rho u)_0](\rho U)_0 \\ [(\rho v)_0 + a_q (\rho v)'](U)' \\ \quad + [(\rho v)' - (\rho'/\rho_0)(\rho v)_0](\rho U)_0 \\ [(\rho E + p)_0 + a_q (\rho E + p)'](\rho U)' \\ \quad + [(\rho E + p)' - (\rho'/\rho_0)(\rho E + p)_0](\rho U)_0 \end{bmatrix} \tag{12}$$

$$\hat{F} = \begin{bmatrix} (\rho V)' \\ -y_\xi p' \\ +x_\xi p' \\ 0 \end{bmatrix} + \frac{1}{(\rho_0 + a_q \rho')} \begin{bmatrix} 0 \\ [(\rho u)_0 + a_q (\rho u)'](\rho V)' \\ \quad + [(\rho u)' - (\rho'/\rho_0)(\rho u)_0](\rho V)_0 \\ [(\rho v)_0 + a_q (\rho v)'](\rho V)' \\ \quad + [(\rho v)' - (\rho'/\rho_0)(\rho v)_0](\rho V)_0 \\ [(\rho E + p)_0 + a_q (\rho E + p)'](\rho V)' \\ \quad + [(\rho E + p)' - (\rho'/\rho_0)(\rho E + p)_0](\rho V)_0 \end{bmatrix} \tag{13}$$

where

$$p' = (\gamma - 1)\left((\rho E)' - \frac{1}{(\rho_0 + a_q \rho')}\left\{\left[(\rho u)_0 + \frac{a_q}{2}(\rho u)'\right](\rho u)' + \left[(\rho v)_0 + \frac{a_q}{2}(\rho v)'\right](\rho v)' - \frac{\rho'}{2\rho_0}[(\rho u)_0^2 + (\rho v)_0^2]\right\}\right) \tag{14}$$

III. Numerical Solution Procedure

The governing equations (9) are solved by an explicit four-stage Runge-Kutta time-marching finite-volume numerical scheme that has been successfully employed by Jameson et al.[7] for the solution of the Euler equations. The salient features of this finite-volume procedure are briefly described in the following section.

A. Finite-Volume Discretization

The spatial computational domain is first divided into quadrilateral cells bounded by straight lines (Fig. 1). The flowfield variables are computed at the center of each cell, and a system of ordinary differential equations in time is obtained by integrating over each cell area as follows:

$$\iint_A \frac{\partial}{\partial t}(J\hat{q}')\,dA + \iint_A \left(\frac{\partial \hat{E}'}{\partial \xi} + \frac{\partial \hat{F}'}{\partial \eta}\right) dA = \iint_A S_a\,dA \tag{15}$$

The second double integral over the entire area of the cell can easily be transformed to the single integral around the boundaries of the cell (representing influx or outflux) by means of Green's theorem. In many cases, the right-hand double integral containing the source terms can also be represented by the line integral around the boundaries of the cell. Thus there are two options to model the source field. Either the source field can be modeled by inhomogeneous inflow boundary conditions with $S_a = 0$, or it can have homogeneous inflow boundary conditions with inhomogeneous equations reflecting the effects of the sources. However, the examples presented in this paper have been computed using the first option. Furthermore, there are two ways to incorporate the inhomogeneous boundary conditions resulting from the source field. Either the flux due to the source can be prescribed at the boundaries of the cell containing the source, or the entire acoustic field can be considered as being composed of the field of the acoustic source plus a superimposed field generated as a result of the presence of the solid boundaries. In the latter case only the superimposed field needs to be solved. However, the wall boundary conditions must be modified in order to take into account the effects of the source field. In the present computations, the second approach has been adopted. The modified wall-boundary conditions are explained in the next section.

Thus in all our cases the right-hand integral vanishes. If the flowfield variables associated with the cell (i,j) are represented by the subscript (i,j), then the finite-volume discretization of Eq. (15) will be given by

$$\frac{d}{dt}(J_{ij}\hat{q}'_{ij}) + (\hat{E}_{i+\frac{1}{2},j} - \hat{E}'_{i-\frac{1}{2},j}) + (\hat{F}_{i,j+\frac{1}{2}} - \hat{F}_{i,j-\frac{1}{2}}) = \tilde{S}_{a_{i,j}} \tag{16}$$

Note that the fluxes at each face of a cell are computed by taking the average values of the flow variables corresponding to the cells that have the face in common. Suppressing the subscripts, Eq. (16) can also be written as

$$\frac{d(J\hat{q}')}{dt} + F\hat{q}' = 0 \tag{17}$$

where the operator F represents the convective and source terms.

B. Artificial Dissipative Terms

The finite-volume scheme is augmented with the additional fourth-order artificial dissipative terms in order to suppress the tendency for odd- and even-point decoupling and to prevent the appearance of high-frequency numerical oscillations in the flowfields. The details regarding these terms can be found elsewhere (e.g., Jameson et al., Ref. 7). However, briefly stated, Eq. (17) has been replaced by the following equation:

$$\frac{d(J\hat{q}')}{dt} + F\hat{q}' - D\hat{q}' = 0 \tag{18}$$

where D is the dissipative operator that consists of the following operators in each direction:

$$D\hat{q}' = D_x\hat{q}' + D_y\hat{q}' \tag{19}$$

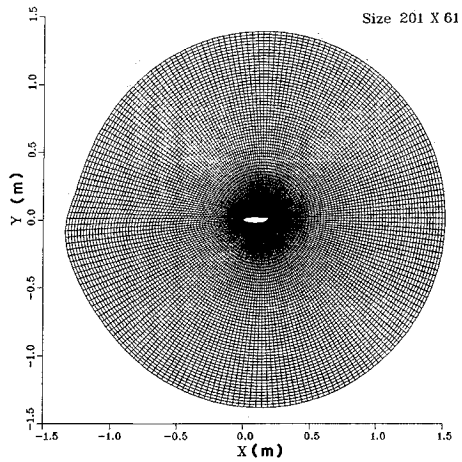

Fig. 4a The computational grid for GA(W)-1 airfoil.

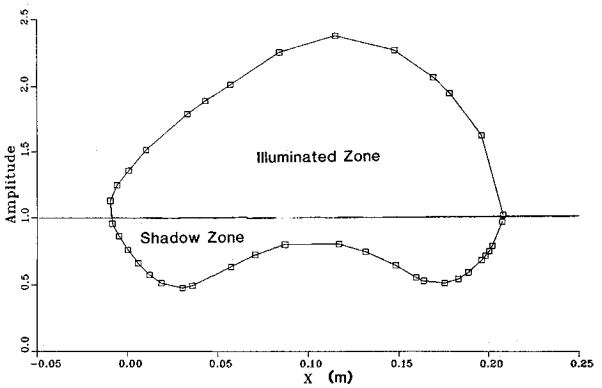

Fig. 4b The acoustic pressure in the vicinity of the airfoil surface due to the diffraction of the plane waves by GA(W)-1 airfoil.

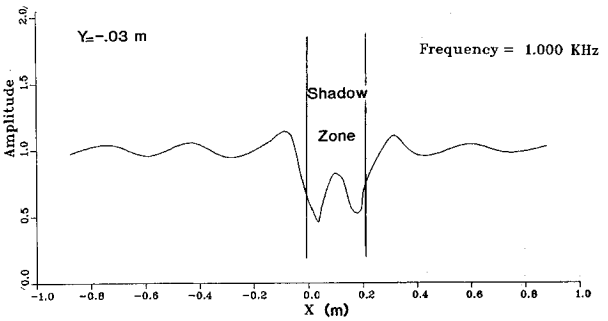

Fig. 4c The acoustic pressure along the line $y = -0.03$ m under the airfoil surface due to the diffraction of the plane waves by GA(W)-1 airfoil.

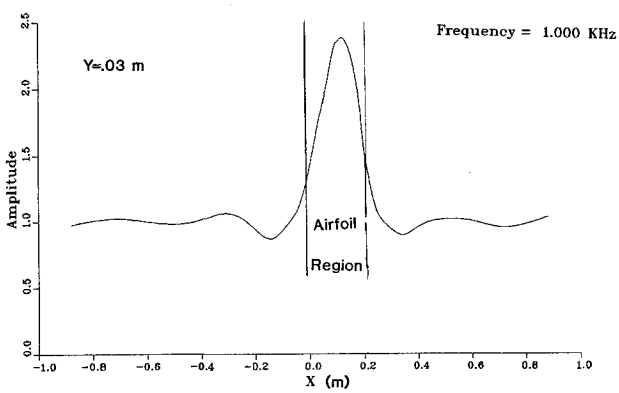

Fig. 4d The acoustic pressure along the line $y = 0.03$ m above the airfoil surface due to the diffraction of the plane waves by GA(W)-1 airfoil.

The dissipative fluxes in each direction are given by

$$D_x\hat{q}' = d_{i+\frac{1}{2},j} - d_{i-\frac{1}{2},j}$$

$$D_y\hat{q}' = d_{i,j+\frac{1}{2}} - d_{i,j-\frac{1}{2}} \tag{20}$$

where

$$d_{i+\frac{1}{2},j} = -\epsilon \frac{j_{i+\frac{1}{2},j}}{\Delta t}(\hat{q}'_{i+2,j} - 3\hat{q}'_{i+1,j} + 3\hat{q}'_{i,j} - \hat{q}'_{i-1,j})$$

The other terms $d_{i,j+\frac{1}{2}}$, $d_{i,j-\frac{1}{2}}$, etc. are calculated in an analogous manner. The numerical value of the constant ϵ influences the solution's accuracy and hence must be carefully selected. The typical value of the constant ϵ is 1/32.

C. Runge-Kutta Time-Stepping Scheme

The integration of the ordinary differential Eq. (18) is performed in time using the classical four-stage Runge-Kutta scheme. At each time step, the scheme employs four stages as follows:

$$\hat{q}^{(0)} = \hat{q}'^{(n)}$$

$$\hat{q}^{(1)} = \hat{q}^{(0)} - \frac{\Delta t}{8}(F\hat{q}^{(0)} - D\hat{q}^{(0)})$$

$$\hat{q}^{(2)} = \hat{q}^{(0)} - \frac{\Delta t}{6}(F\hat{q}^{(1)} - D\hat{q}^{(0)})$$

$$\hat{q}^{(3)} = \hat{q}^{(0)} - \frac{\Delta t}{4}(F\hat{q}^{(2)} - D\hat{q}^{(0)})$$

$$\hat{q}^{(4)} = \hat{q}^{(0)} - \frac{\Delta t}{2}(F\hat{q}^{(3)} - D\hat{q}^{(0)})$$

$$\hat{q}'^{(n+1)} = \hat{q}^{(4)} \tag{21}$$

In this scheme, the dissipative terms are frozen at their values in the first stage in order to avoid expensive computations in each stage. The scheme has been found stable for Courant numbers $\leq 2\sqrt{2}$ by various investigators (e.g., Ref. 7) for the Euler equations. In the present case, the maximum time step is determined by the resolution of the highest desired frequency. This time step usually corresponds to a much lower Courant number than that dictated by stability limits.

IV. Boundary Conditions

The preceding formulated numerical scheme holds for arbitrary steady mean flows. It is implicit in the formulation that the steady mean flow is already known by the application of a standard Euler solver such as that developed by Jameson et al.[7] The capability of the scheme to accurately predict the acoustic fields associated with the radiation due to a monopole in a freefield, near a plane wall, in a uniform stream, or inside a jet has been demonstrated by Khan.[9] In the present paper, the scheme has been applied to predict the diffracted acoustic field around realistic geometrical configurations in the absence of mean flow. Thus in this paper we restrict ourselves to boundary conditions applicable to the diffraction problems in stationary media. All of the boundary conditions are implemented explicitly as described in the following subsections.

A. Far-Field Radiation Boundary Conditions

Since it is not practical to use an infinite domain for computations, one must truncate the domain with an artificial boundary and impose conditions on this surface to simulate an infinite domain. It is, therefore, desirable that there should be no reflections from the boundary back into the

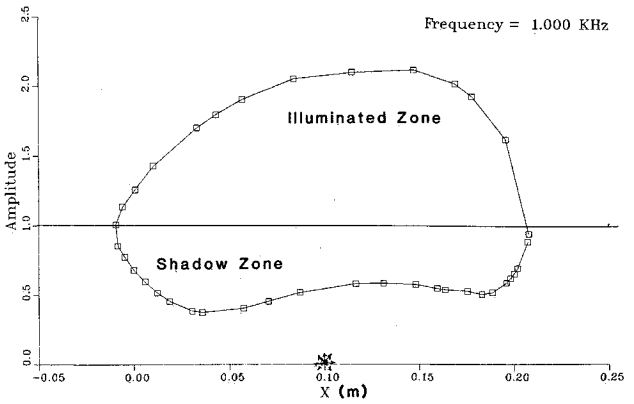

Fig. 5a The acoustic pressure in the vicinity of the airfoil surface due to the diffraction of a monopole field by GA(W)-1 airfoil.

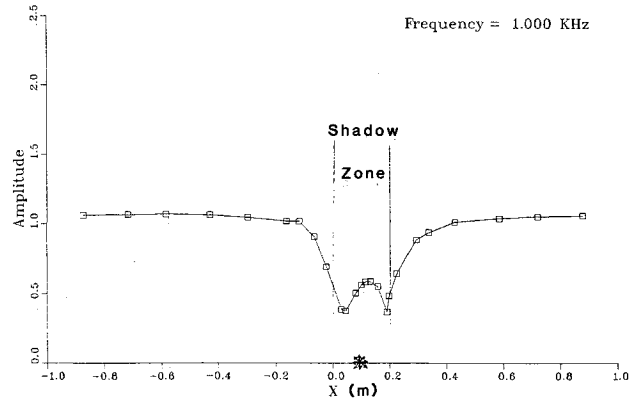

Fig. 5b The acoustic pressure along the line $y=-0.03$ m under the airfoil surface due to the diffraction of a monople field by GA(W)-1 airfoil.

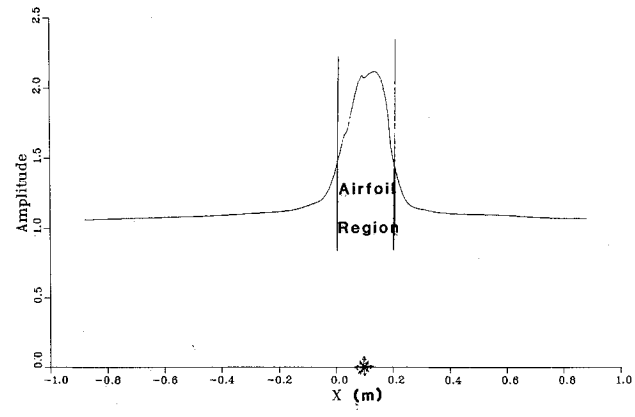

Fig. 5c The acoustic pressure along the line $y=0.03$ m above the airfoil surface due to the diffraction of a monople field by GA(W)-1 airfoil.

domain of interest. Various investigators (such as Rudy and Strikwerda[10] and the references contained therein) have developed different sets of nonreflecting boundary conditions. Although these boundary conditions are found to accelerate Navier-Stokes solutions to the steady state, most of them do not take into account the correct behavior of the solution far from the body. Bayliss and Turkel[11] have constructed a family of radiation boundary conditions based on an asymptotic expansion of the solution of the Helmholtz equation, valid for large distances. Thus, the applied far-field condition is the first member of this family. This condition for the acoustic pressure is given by

$$\frac{\partial p'}{\partial t}+\frac{\partial p'}{\partial r}+\frac{p'}{2r}=0 \tag{22}$$

where

$$r=\sqrt{(x-x_0)^2+(y-y_0)^2} \tag{23}$$

and (x_0,y_0) are the coordinates of the acoustic source. In curvilinear coordinates, it can be written as follows:

$$\frac{\partial p'}{\partial r}=p'_x\cos\alpha+p'_y\sin\alpha$$

$$=J^{-1}[p'_\xi(y_\eta\cos\alpha-x_\eta\sin\alpha)+p'_\eta(-y_\xi\cos\alpha+x_\xi\sin\alpha)]$$

or

$$\frac{\partial p'}{\partial t}+J^{-1}[p'_\xi(y_\eta\cos\alpha-x_\eta\sin\alpha)$$

$$+p'_\eta(-y_\xi\cos\alpha+x_\xi\sin\alpha)]+\frac{p'}{2r}=0 \tag{24}$$

where

$$\tan\alpha=(y-y_0)/(x-x_0)$$

Thus, the fluctuating pressure is computed from the preceding equation. Then the fluctuating density is obtained by assuming an isentropic relation at infinity. The velocity component fluctuations are obtained by the ξ,η momentum equations applied at infinity, i.e.,

$$\frac{\partial u'}{\partial t}=-\frac{\partial p'}{\partial x}=J^{-1}[p'_\xi y_\eta-p'_\eta y_\xi]$$

$$\frac{\partial v'}{\partial t}=-\frac{\partial p'}{\partial y}=J^{-1}[-p'_\xi x_\eta+p'_\eta x_\xi] \tag{25}$$

and the energy fluctuations are then obtained from Eq. (14).

B. Wall Boundary Conditions

Time-accurate wall boundary conditions are necessary for the accurate prediction of the near field. In the present paper, the acoustic field is computed as the acoustic field of the source plus a superimposed acoustic field resulting from the existence of the solid boundaries. The numerical scheme is then employed only to compute the superimposed field. The superimposition requires the modification of the wall boundary conditions as has been explained in the previous section. Since the flow is inviscid, the contravariant velocity component normal to the wall must vanish. Employing this concept, one can obtain the wall boundary conditions as follows.

Denoting the source field by subscript s and the superimposed field by subscript r, the condition to enforce at the wall must be

$$(\rho V)'\equiv 0\equiv(\rho V)'_s+(\rho V)'_r \tag{26}$$

Therefore, in the absence of mean flow the two acoustic momentum equations embedded in Eq. (9) can be simplified to yield the following:

$$\frac{\partial p'_r}{\partial\eta}=\left[\frac{y_\eta y_\xi+x_\eta x_\xi}{x_\xi^2+y_\xi^2}\right]\frac{\partial p'_r}{\partial\xi}-\frac{1}{(x_\xi^2+y_\xi^2)}\frac{\partial}{\partial t}[J(\rho V)'_s] \tag{27a}$$

$$\frac{\partial[J(\rho U)'_r]}{\partial t}=\frac{J^2}{(x_\xi^2+y_\xi^2)}\cdot\frac{\partial p'_r}{\partial\xi}-\left(\frac{y_\eta y_\xi+x_\xi x_\eta}{x_\xi^2+y_\xi^2}\right)\frac{\partial[J(\rho V)'_s]}{\partial t} \tag{27b}$$

Equations (27) are employed to determine p', $(\rho U)'$ at the wall, the fluctuating density is computed from the isentropic relation, and the fluctuating velocity components are computed by using Eqs. (11) as follows:

$$(\rho u)' = J^{-1} x_\xi (\rho U)', \quad (\rho v)' = J^{-1} y_\xi (\rho U)' \tag{28}$$

V. Results

The computational method has been applied to solve the problems of diffraction of sound waves. A few diffraction problems of known analytical solutions have been selected in order to validate the code. The computations are performed by marching in the time domain, starting with no acoustic-field condition inside the computational domain. As the time is progressed, the solution is monitored in order to make sure that the transient state of the solution has been passed and that it has reached an oscillatory state. In each of the cases described in the following sections, some discrete points of interest are selected in the space at which the Fourier-Transform of the pressure fluctuations for the frequencies of interest has been computed by accumulating them at each time step. The resulting acoustic-pressure amplitudes are then plotted.

A. Diffraction of Plane Waves by a Knife Edge

This example serves as an excellent test case for demonstrating the prediction capability of the present computational method for the diffraction of the plane waves. The acoustic field has been computed by using a 181×181 square grid. Plane waves having a frequency of 5.0 KHz are impinging upon a knife edge which is parallel to the y axis, as shown schematically in Fig. 2. The resulting pressure amplitudes are plotted along a line parallel to the knife edge located at $kx = 24.83$. The results are found to be in excellent agreement with the exact analytical solution (shown by a solid line) which is given by Morse and Ingard[12] in terms of Fresnel integrals. The interaction of the incident and the diffracted waves has been predicted very well in both the shadow and the illuminated regions.

B. Diffraction of Plane Waves by a Circular Cylinder

Another example of the known analytical solution is the diffraction of the plane waves impinging upon a cylinder. The acoustic field has been considered as being composed of the acoustic field due to the plane waves and a superimposed field resulting from the presence of the cylinder. Then the superimposed field has been computed by using a 100×30 polar grid shown in Fig. 3a. The central white area in the figure indicates a cylinder of a diameter of 10 cm. Plane waves having a frequency of 1 KHz are impinging upon the cylinder from the left in the x direction. The combined results are plotted in Figs. 3b–3e in the vicinity of the cylinder, along lines $kr = 1.08, 3.59, 6.72$, and 9.23, respectively. The results are plotted against the analytical solution (shown with a solid line) given by Morse and Ingard[12] as a series of Bessel functions. The numerical results are found to be in excellent agreement with the analytical solution. Both the reflection and the diffraction of the plane waves by the cylinder have been predicted very well.

C. Diffraction of Plane Waves by the GA(W)-1 Airfoil

The diffraction of plane waves by an airfoil forms a problem of practical importance. It can be used in assessing the shielding capability of an airfoil. In this case, the computational method has been applied for solving the diffraction of plane waves by the GA(W)-1 airfoil. The acoustic field has been computed using a 201×61 O-grid shown in Fig. 4a. The center white area in the figure indicates the airfoil as having a chord length of 0.208 m. Plane waves having a frequency of 1 KHz are impinging upon the airfoil from the top in the negative y direction. The results are plotted in Fig. 4b–4d in the vicinity of the airfoil along lines $y = 0.03$ m and -0.03 m, respectively. The results indicate that in the illuminated zone, the maximum pressure amplitude occurs near the midchord of the airfoil. The pressure amplitudes in the shadow zone, however, indicate that maximum shielding region splits into two parts that remain concentrated under the leading and the trailing edges.

D. Diffraction of the Acoustic Field of a Monopole by GA(W)-1 Airfoil

In this case, the computational method has been applied for solving the diffraction of the acoustic field of a monopole by the GA(W)-1 airfoil. The monopole having a frequency of 1KHz is located at a distance of 0.10 m from the leading edge and at a height of 0.11 m above the airfoil. The acoustic field has been computed by using the same grid as in the preceding case. The results are plotted in Figs. 5 in the vicinity of the airfoil along lines $y = 0.03$ m and -0.03 m respectively in terms of the pressure amplitudes relative to those without the airfoil. The results exhibit features similar to those in the case of the diffraction of the plane waves. In this case also, the pressure amplitudes in the shadow zone indicate that the maximum shielding region splits into two parts under the airfoil. However, the pressure amplitudes approach the freefield values smoothly away from the airfoil.

VI. Conclusion

The problem of the diffraction of acoustic waves by rigid cylindrical bodies of arbitrary cross sections has been solved by developing and applying a computational method in the field of aeroacoustics. The solution has been obtained by solving the fundamental inviscid equations of aeroacoustics using a time-marching finite-volume technique. The prediction capability of the method has been demonstrated by testing it against the known cases of the diffraction of the plane waves by a knife edge and a cylinder. The method has predicted the acoustic field resulting from the interaction of the incident, reflected, and diffracted fields very well in both the shadow and the illuminated zones. The method forms a fundamental tool for solving realistic problems of diffraction and has been successfully applied to compute practical problems such as the diffraction of plane waves and of a monopole acoustic field by a GA(W)-1 airfoil.

Acknowledgment

This work was done under Lockheed-Georgia's Independent Research and Development program.

References

[1]Hardin, J. C. and Lamkin, S. L., "Aeroacoustic Computation of Cylinder Wake Flow," *AIAA Journal*, Vol. 22, Jan. 1984, pp. 51–57.

[2]Pao, S. P. and Salas, M. D., "A Numerical Study of Two-Dimensional Shock Vortex Interaction," AIAA Paper 81-1205, 1981.

[3]Hariharan, S. I. and Bayliss, A., "Radiation of Sound from Unflanged Cylindrical Ducts," *SIAM Journal on Scientific and Statistical Computing*, Vol. 6, 1985, pp. 285–296; also, NASA Contractor Rept. 172171, ICASE, July 1983.

[4]Hariharan, S. I., "Numerical Solutions of Acoustic Wave Propagation Problems Using Euler Computations," AIAA Paper 84-2290, 1984; also, NASA Contractor Rept. 172434, ICASE Rept. 84-39, Aug. 1984.

[5]Fasel, H., "Investigation of the Stability of Boundary Layers by a Finite-Difference Model of the Navier-Stokes Equations," *Journal of Fluid Mechanics*, Vol. 78, Pt. 2, 1976, pp. 355–383.

[6]Bayliss, A., Goldstein, C. I., and Turkel, E., "On Accuracy Conditions for the Numerical Computation of Waves," *Journal of Computational Physics*, Vol. 59, 1985, pp. 390–404; also, NASA Contractor Rept. 172433, ICASE Rept. 84-38, Aug. 1984.

[7]Jameson, A., Schmidt, W., and Turkel, E., "Numerical Solutions of the Euler Equations by Finite Volume Methods Using Runge-Kutta Time-Stepping Schemes," AIAA Paper 81-1259, 1981.

[8]Pulliam, T. H. and Steger, J. L., "Implicit Finite-Difference Simulations of Three-Dimensional Compressible Flow," *AIAA Journal*, Vol. 18, Feb. 1980, pp. 159-167.

[9]Khan, M. M. S., "Computations of Aeroacoustic Fields Using Finite Volume Method," *Proceedings of the First IMACS Symposium on Computational Acoustics*, edited by D. Lee, R. L. S. Fernberg, and M. H. Schultz, Yale Univ., New Haven, CT, Aug. 1986.

[10]Rudy, D. H. and Strikwerda, J. C., "A Nonreflecting Outflow Boundary Condition for Subsonic Navier-Stokes Calculations," *Journal of Computational Physics*, Vol. 36, 1980, pp. 55-70.

[11]Bayliss, A. and Turkel, E., "Radiation Boundary Conditions for Wave-Like Equations," *Communications on Pure and Applied Mathematics*, Vol. 33, 1980, pp. 707-725.

[12]Morse, P. M. and Ingard, K. U., "Theoretical Acoustics," McGraw-Hill, New York, 1968.